Title: Suppression of Sleep Spindle Rhythmogenesis in Mice with Deletion of CaV3.2 and CaV3.3 T-type Ca(2+) Channels.

Authors: Pellegrini C, Lecci S, Lüthi A, Astori S

Journal: Sleep

Year: 2016 Apr 1

Volume: 39

Issue: 4

Pages: 875-85

DOI: 10.5665/sleep.5646

Suppression of sleep spindle rhythmogenesis in mice with deletion of $Ca_V3.2$ and $Ca_V3.3$ T-type Ca^{2+} channels

Chiara Pellegrini, MSc; Sandro Lecci, MSc ; Anita Lüthi, PhD; Simone Astori, PhD

Department of Fundamental Neurosciences, University of Lausanne, Rue du Bugnon 9, CH-1005 Lausanne, Switzerland.

[1]Corresponding authors: Simone Astori, PhD; Anita Lüthi, PhD

Department of Fundamental Neurosciences,
University of Lausanne,
Rue du Bugnon 9
CH-1005 Lausanne
Phone: +41 21 692 5294
Fax: +41 21 692 5105
E-mail: simone.astori@unil.ch; anita.luthi@unil.ch

Number of pages: 22
Number of figures: 6
Number of tables: 0
Number of words in abstract: 250

DISCLOSURE STATEMENT

This was not an industry supported study. The authors declare no financial conflict of interests.

RUNNING HEAD

Ca_V3 double-deletion suppresses sleep spindles

ABSTRACT

Study objectives Low-threshold voltage-gated T-type Ca^{2+} channels (T-channels or Ca_V3 channels) sustain oscillatory discharges of thalamocortical (TC) and *nucleus Reticularis thalami* (nRt) cells. The $Ca_V3.3$ subtype dominates nRt rhythmic bursting and mediates a substantial fraction of spindle power in the NREM sleep EEG. $Ca_V3.2$ channels are also found in nRt, but whether these contribute to nRt-dependent spindle generation is unexplored. We investigated thalamic rhythmogenesis in mice lacking this subtype in isolation ($Ca_V3.2$KO mice) or in concomitance with $Ca_V3.3$ deletion (Ca_V3.double-knockout (DKO) mice).

Design We examined discharge characteristics of thalamic cells and intrathalamic evoked synaptic transmission in brain slices from wild-type, $Ca_V3.2$KO and Ca_V3.DKO mice by patch-clamp recordings. The sleep profile of freely-behaving Ca_V3.DKO mice was assessed by polysomnographic recordings.

Measurements and Results $Ca_V3.2$ channel deficiency left nRt discharge properties largely unaltered, but additional deletion of $Ca_V3.3$ channels fully abolished low-threshold whole-cell Ca^{2+} currents and bursting, and suppressed burst-mediated inhibitory responses in TC cells. Ca_V3.DKO mice had more fragmented sleep, with shorter NREM sleep episodes and more frequent microarousals. NREM sleep EEG power spectrum displayed a relative suppression of the σ frequency band (10-15 Hz), which was accompanied by an increase in the δ band (1-4 Hz).

Conclusions Consistent with previous findings, $Ca_V3.3$ channels dominate nRt rhythmogenesis, but the lack of $Ca_V3.2$ channels further aggravates neuronal, synaptic and EEG deficits. Therefore, $Ca_V3.2$ channels can boost intrathalamic synaptic transmission, and might play a modulatory role in the relative presence of NREM sleep EEG rhythms.

Keywords sleep spindles, sleep architecture, nucleus Reticularis thalami

INTRODUCTION

Low voltage-gated T-type Ca^{2+} channels (T-channels) enable neurons to produce low-threshold discharges that are essential for the generation of sleep rhythms,[1-3] but that occur also in motor control[4, 5] and olfaction.[6] Furthermore, T-channels may lead to aberrant bursting in neurons exposed to abnormal electrical activity.[1, 7, 8] T-channels are encoded by three genes, *CACNA1g*, *CACNA1h* and *CACNA1i* that give rise to the subtypes $Ca_V3.1$, $Ca_V3.2$ and $Ca_V3.3$, respectively, characterized by different biophysical properties and expression patterns.[9, 10] T-channels are most abundant in thalamus, where they exhibit regional specificity: whereas $Ca_V3.1$ channel mRNA is restricted to excitatory thalamocortical (TC) cells, e.g. in the ventrobasal nucleus (VB), mRNA for both $Ca_V3.2$ and $Ca_V3.3$ channels is present in the *nucleus Reticularis thalami* (nRt),[10, 11] a shell of GABAergic cells modulating the information flow in the thalamocortical system.[12]

Genetic manipulations of Ca_V3 channels have yielded substantial insight into the mechanisms of oscillatory activity of neuronal cells. However, in contrast to the well-established role of T-channels in single-cell burst discharge, how these channels contribute to network rhythmic activity has only partially progressed since the generation of knock-out (KO) animals. Furthermore, in at least some cases, the relation between the cellular effects of T-channel subtype deletion and the purported role of burst discharges in EEG rhythms remains obscure. For example, $Ca_V3.1$ channels are clearly responsible for low-threshold bursting in TC cells. However, both increases and decreases in the δ power (1-4 Hz) of the NREM sleep EEG were observed in animals lacking $Ca_V3.1$ channels.[13, 14] Therefore, a long-standing tenet on the TC cell clock-like burst discharges as basis for the EEG δ rhythm[15, 16] could not yet be confirmed based on Ca_V3 channel genetics.

We have previously shown that the $Ca_V3.3$ subtype is the major source of low-threshold Ca^{2+} spikes in nRt cell dendrites.[17] In $Ca_V3.3$KO mice, nRt repetitive burst discharges were strongly reduced, leading to an impaired inhibitory drive onto TC cells. Furthermore, consistent with the previously recognized implication of the nRt in sleep spindle pacemaking, EEG power in the σ frequency range (10-15 Hz) was weakened at transitions between NREM and REM sleep in $Ca_V3.3$KO animals. There were no other

major changes in EEG frequency bands, which indicated a $Ca_V3.3$-specific decrease in sleep spindle rhythmogenesis.[17]

Although $Ca_V3.3$-deficiency led to a reduction in sleep spindles, a substantial portion of power increase remained present in the σ frequency band at NREM sleep exit, suggesting that other cellular mechanisms contributing to these thalamocortical rhythms exist. A major candidate is the $Ca_V3.2$-current that has been identified in nRt cells,[18] and that appears to be the target of several modulatory extracellular and intracellular signaling molecules.[19] To date, $Ca_V3.2$ channels are implicated in peripheral nociception and neuropathic pain, and might be involved in specific forms of thalamic processing, e.g. relay of nociceptive inputs.[20-22] In addition, the expression of $Ca_V3.2$ channels can be modified in pathological conditions, e.g. in animal models of epilepsy.[7] Whether and how $Ca_V3.2$ channels contribute to thalamic sleep rhythmogenesis has yet not been ascertained.

Here, we examined the consequences of silencing Ca_V3-mediated nRt rhythmogenesis on the EEG profile of mice harboring a deletion of *$Ca_V3.2$* and *$Ca_V3.3$* genes (Cav3.DKO). Whereas lack of the $Ca_V3.2$ subtype alone in $Ca_V3.2$KO mice did not cause major alterations to nRt cellular properties, Ca_V3.DKO mice showed a fully abolished nRt low-threshold spiking and strongly impaired intrathalamic GABAergic transmission. In freely-behaving Ca_V3.DKO mice, relative EEG power in the σ frequency range during NREM sleep was suppressed and accompanied by an increase in the δ frequency range. Although Ca_V3.DKO mice spent globally more time in NREM sleep during the light phase, NREM sleep episodes were of shorter duration compared to wild-type animals. Thus, silencing low-threshold bursts in nRt neurons not only affects spindle generation, but also alters slow-wave rhythmogenesis, likely due to deficient inhibitory drive onto TC cells.

MATERIALS AND METHODS

Animal handling and genotyping

All procedures were approved by the Veterinary Office of the Canton de Vaud. C57Bl/6J (wild-type), $Ca_V3.2$KO and Ca_V3.DKO mice were maintained under a 12:12h light/dark schedule (lights on at 7AM for animals used for electrophysiological recordings; lights on at 9AM for polysomnographic

recordings). Ca_V3.DKO mice were obtained by crossing the $Ca_V3.2$KO (C57Bl/6J-Cacna1h-KO) and $Ca_V3.3$KO (C57Bl/6J-Cacna1i-KO) mouse lines, with subsequent selection of breeding pairs with the genetic background $Ca_V3.2$*het*/$Ca_V3.3$KO. The genotype was determined by PCR using the following primers (5'-3') for the *CACNA1h* gene: CACNA1hF: ATTCAAGGGCTTCCACAGGGTA; CACNA1hR: CATCTCAGGGCCTCTGGACCAC; CACNA1hNeo: GCTAAAGCGCATGCTCCAGACTG, yielding products of 480 bp for wild-type and 330 bp for $Ca_V3.2$KO mice.[23] For the *CACNA1i* gene, primers were: CACNA1iF: CTGCTGTGGTACCCTCCTGTC; CACNA1iR: GACAGGGTACCTGCTGCATG; EN-2SA-3R: GGGTTCGTGTCCTACAACAC, yielding products of 900 bp for wild-type and 545 bp for $Ca_V3.3$KO mice.

Electrophysiological recordings and analyses

Acute horizontal brain slices (300 µm-thick) were prepared from 3-4 week-old animals of either sex, as previously described.[17, 24] In the recording chamber, slices were constantly superfused with oxygenated artificial CSF (ACSF) at 30-32°C containing (in mM): 125 NaCl, 25 $NaHCO_3$, 2.5 KCl, 1.25 NaH_2PO_4, 1.2 $MgCl_2$, 2 $CaCl_2$, 25 glucose, 1.7 L(+)-ascorbic acid. Visually identified nRt and TC neurons were whole-cell patched with borosilicate glass pipettes (TW150F-4, WPI). For recordings of passive membrane properties and spike discharges, pipettes (3-5 MΩ) were filled with an intracellular solution containing (in mM): 140 $KMeSO_4$, 10 KCl, 10 HEPES, 0.1 EGTA, 4 Mg-ATP, 0.2 Na-GTP, 10 phosphocreatine (290-300 mOsm, pH 7.25). A liquid junction potential of -10 mV was taken into account. For T-current isolation, patch pipettes (2-3 MΩ) were filled with the following solution (in mM): 135 tetramethylammonium hydroxide (TMA-OH), 40 HEPES, 10 EGTA, 2 MgCl2, 4 Mg-ATP, titrated to pH 7.2 with hydrofluoric acid (HF). The extracellular solution was supplemented with 1 µM tetrodotoxin. A liquid junction potential of -2 mV was corrected for. T-current density and activation curve were estimated as previously described.[17] For IPSC recordings in TC cells, pipettes (3-4 MΩ) were filled with (in mM): 127 CsGluconate, 10 HEPES, 2 BAPTA, 6 $MgCl_2$, 2 Mg-ATP, 0.2 Na-GTP, 10 phosphocreatine, 2.5 QX-314 (290-300 mOsm, pH 7.25). In TC neurons voltage-clamped at -30 mV, postsynaptic responses were evoked by monopolar stimulation in the internal capsule with an ACSF-

filled glass electrode, in the absence of glutamatergic blockers. IPSC charge transfer was calculated as the integral of the current trace during 1s from response onset.

Series resistance (R_s) was monitored throughout recordings by brief voltage pulses, and data were rejected for R_s changes >25%. Data were acquired through a Digidata1320 digitizer. Signals were amplified through a Multiclamp700B amplifier (Molecular Devices), sampled at 20 kHz and filtered at 10 kHz using Clampex10 (Molecular Devices). Clampfit10 (Molecular Devices) and Igor Pro 6 (WaveMetrics) were used for data analysis.

Chemicals

All standard salts and chemicals were purchased from SigmaAldrich, except the following: $KMeSO_4$ (ICN Biomedicals); L(+)-ascorbic acid (VWR Prolabo); Tetrodotoxin, (Latoxan); QX-314-Cl (Alomone Labs).

Polysomnographic recordings and analyses

Electroencephalographic (EEG/ECoG) and electromyographic (EMG) recordings were performed in male Ca_V3.DKO mice and wild-type mice chronically implanted with electrodes for differential fronto-parietal EEG and nuchal muscle EMG, as previously described.[17, 25] At the time of surgery, animals were 6-9 weeks old. Ca_V3.DKO mice had lower body weights (wild-type: 22.3 ± 0.9 g, n = 8 vs. Ca_V3.DKO: 19.3 ± 0.9 g, n = 8; $P < 0.05$, unpaired *t*-test). During one week of post-surgery recovery, mice received paracetamol (2 mg/ml) in drinking water. Animals were allowed one additional week to habituate once electrode implants were connected to the tethering cables. Polysomnographic acquisitions were performed in 48 h-long sessions with groups of four animals. The analog EEG and EMG signals were first amplified (gain 2000 x), and then high-pass filtered at 0.7 Hz and 10 Hz, respectively. Data were digitized at 2 kHz and down-sampled to 200 Hz through Somnologica 3.3.1 software (Embla System). Vigilance states were visually scored as wakefulness, NREM or REM sleep based on EEG/EMG signals according to well-established criteria.[25] Power spectra were determined from 48 h-long recordings using discrete-Fourier transformation between 0.75 to 90 Hz (0.25 Hz bins) for consecutive 4 s-epochs. For spectral analysis, a given epoch was rejected when an adjacent epoch was scored to a different vigilance

state or contained movement artifacts. On average, 74 ± 5% of the total waking time, 93 ± 1% of the total NREM sleep time and 75 ± 2% of the total REM sleep time were included in the spectral analysis of wild-type animals, and 74 ± 7%, 91 ± 1% and 76 ± 4% of total time in the corresponding behavioral state were included for Ca_V3.DKO mice. Mean power spectra were calculated as the average of all artifact-free 4 s-epochs of the corresponding vigilance state during both light and dark phase. Sigma power at NREM-to-REM sleep transition was determined according to previously described procedures.[17, 25] Microarousals were defined as waking episodes of ≤16 s duration preceded and followed by at least five and four NREM sleep episodes, respectively. EEG analyses were performed with customized semi-automated routines written in Matlab v8.5 R2015a (The Mathworks).

Statistical Analyses

Data are presented as mean ± SEM. The use of parametric on non-parametric statistical tests was supported by checking the normal distribution of the data. One-way ANOVA and repeated measures ANOVA were performed in JMP.10 (SAS Institute Inc.), followed by p*ost hoc* Student's *t*-test, with significance accepted for $P < 0.05$. Greenhouse–Geisser (G-G) correction was applied to account for violation of sphericity (Mauchly's test), where necessary. Cumulative distributions of bouts of behavioral states were compared with the Kolmogorov-Smirnov test in Matlab, with a significance level of 0.05.

RESULTS

Abolishment of nRt low-threshold burst discharges in Ca_V3.DKO mice

In acute brain slices from wild-type, Ca_V3.2KO and Ca_V3.DKO mice, we compared basic electrophysiological parameters of nRt neurons by means of whole-cell patch-clamp recordings (Figure 1). No overt difference between genotypes was present for values of resting membrane potential (V_{rmp}), cell capacitance (C_m) and input resistance (R_i) (wild-type, n = 11 cells; Ca_V3.2KO, n = 9; Ca_V3.DKO, n = 9; P > 0.05, one-way ANOVA; Figure 1A). Current responses to hyperpolarizing voltage steps, which include activation of inwardly rectifying and HCN channels, were also comparable (Figure 1B). Moreover, tonic firing elicited by depolarizing current injections (400 ms) from a holding potential of -70 mV displayed similar input-output relationships (wild-type, n = 9; Ca_V3.2KO, n = 8; Ca_V3.DKO, n = 9; Figure 1C). We noticed a tendency of Ca_V3.DKO neurons to sustain prolonged tonic firing, whereas wild-type and Ca_V3.2KO often displayed strong accommodation after the first 200 ms of depolarization. We quantified spiking frequency during the second half of the 400 ms-long depolarization, and found a marked, yet not statistically significant, difference in Ca_V3.DKO neuron firing rate (e.g. 400 pA step: wild-type, 26.7 ± 17.8 Hz; Ca_V3.2KO, 26.8 ± 10.1 Hz; Ca_V3.DKO, 43.9 ± 11.7 Hz; P > 0.05). This is consistent with a previous study reporting on increased propensity of Ca_V3.DKO nRt cells to generate tonic firing during prolonged step depolarization (>1 s).[26]

We next examined low-threshold spiking generated at the offset of brief hyperpolarizing current steps (Figure 2). Wild-type cells (n = 10) displayed rhythmic low-threshold Ca^{2+} spikes accompanied by bursts of Na^+ action potentials, the number of which varied depending on the initial membrane potential. Typically, bursts discharges were best elicited at V_m values in the range between -70 mV and -55 mV. Interestingly, in nRt cells from Ca_V3.2KO mice, no significant change in repetitive bursting was found (P > 0.05; n = 9; Figure 2C-D). Inter-burst intervals measured for discharges elicited from -70 mV also did not differ between genotypes (wild-type, 168 ± 16 ms, n = 6; Ca_V3.2KO, 181 ± 14 ms, n = 8; P > 0.05, unpaired *t*-test). By contrast, Ca_V3.DKO mice displayed a complete lack of oscillatory low-threshold spiking, as previously reported.[26] Occasionally, a single action potential appeared in

Ca_V3.DKO cells at the offset of hyperpolarizing steps applied from more depolarized membrane potentials (-50 mV, observed in 4 out of 9 cells).

Next, we quantified the contribution of $Ca_V3.2$ channels to isolated low-threshold Ca^{2+} currents (T-currents) that were elicited by increasing depolarizing steps applied to nRt cells voltage-clamped at -100 mV (Figure 3). Compared to wild-type cells, currents from $Ca_V3.2$KO cells displayed a slight prolongation of inactivation kinetics ($\tau_{w,\ decay}$ at -60 mV: wild-type, 58.9 ± 4.5 ms, n = 9; $Ca_V3.2$KO, 83.1 ± 10.9 ms, n = 8; P = 0.07, unpaired *t*-test; Figure 3A), consistent with previous data from younger (2 week-old) $Ca_V3.2$KO mice.[18] Current density and activation curve were otherwise comparable, with no significant modification in the estimated V_{half} (wild-type, -71.1 ± 1.0 ms, n = 9; $Ca_V3.2$KO, -69.8 ± 1.7 mV, n = 8; P > 0.05, unpaired *t*-test; Figure 3B). In Ca_V3.DKO mice, no detectable T-currents were generated across the entire range of voltage steps (n = 9).

Together, deletion of $Ca_V3.2$ and $Ca_V3.3$ channels completely abolished T-currents in nRt cells, with a consequent suppression of repetitive oscillatory low-threshold discharges. The absence of the $Ca_V3.2$ subtype did not induce overt changes in the single-cell electrophysiological profile, confirming the dominant role of $Ca_V3.3$ channels in setting nRt cells responsiveness to somatic voltage fluctuations.[17] However, it is also well-known that the thin nRt cell dendrites hamper proper space-clamp, which prevents the controlled activation of voltage-dependent conductances in distal compartments.[27] This could be one reason for which a $Ca_V3.2$-current component went undetected in our somatic whole-cell recordings.

Impaired intrathalamic GABAergic transmission in Ca_V3.DKO mice

We next examined the impact of $Ca_V3.2$ and $Ca_V3.3$ channel deletion on synaptic transmission and excitability within intrathalamic networks, which are both relevant for sleep rhythm generation.[17, 28] We first verified whether thalamocortical (TC) cells in the ventrobasal nucleus (VB) continue to generate low-threshold discharges via $Ca_V3.1$ channels[13, 14] when their synaptic partners in the nRt are burst-deficient. TC cells from wild-type (n = 9), $Ca_V3.2$KO (n = 6) and Ca_V3.DKO (n = 6) mice displayed

comparable responses to hyperpolarizing current injections, which reliably elicited low-threshold spikes crowned by the same number of action potentials (Figure 4A).

Low-threshold bursting of nRt generates phasic inhibitory currents in TC cells comprising a fast and a slow component, mediated by synaptic and non-synaptic $GABA_A$ receptors, respectively.[28, 29] We evoked IPSCs in TC cells held at -30 mV by electrically stimulating the internal capsule, while leaving excitatory transmission intact. In wild-type mice, these typically consisted of multiphasic 'burst IPSCs' (bIPSCs) at stimulation intensities >100 μA, with a sequence of fast events riding on a slower current envelope, as previously reported.[17, 28, 30] Deletion of $Ca_V3.2$ channels decreased the charge transfer of bIPSCs elicited at higher intensities (250-300 μA: wild-type, 91.0 ± 21.1 pC, n = 7; $Ca_V3.2$KO, 50.7 ± 10.7 pC, n = 8; $P < 0.05$ one-way ANOVA; Figure 4B). By contrast, in TC cells from Ca_V3.DKO, only monophasic IPSCs lacking the waveform typical for bIPSCs could be evoked, and the charge transfer was strongly diminished (250-300 μA: Ca_V3.DKO, 13.5 ± 3.6 pC, n = 7; $P < 0.01$ compared to wild-type; Figure 4B).

Together, these data unravel a pronounced deficit in the intrathalamic GABAergic transmission in Ca_V3.DKO mice, which is due to an impaired capability of nRt in generating low-threshold discharges. Although the deletion of $Ca_V3.2$ channels did not appear to affect nRt repetitive bursts in response to somatic current injections, $Ca_V3.2$KO mice displayed a reduction in the charge transfer of bIPSCs. This discrepancy between somatically and synaptically elicited bursting suggests that $Ca_V3.2$ deletion affects the efficacy of excitatory inputs in recruiting nRt dendritic Ca^{2+} conductances.

EEG sleep profile of Ca_V3.DKO mice

The lack of low-threshold bursting in nRt cells from Ca_V3.DKO mice predicted a marked deregulation of thalamic sleep rhythmogenesis. In particular, we expected Ca_V3.DKO mice to exhibit deficits in sleep spindle generation, which depends on nRt bursting and on reverberatory activity within the nRt-TC loop.[31-33] We performed polysomnographic recordings in freely-behaving wild-type (n = 8) and Ca_V3.DKO mice (n = 8) chronically implanted with EEG/EMG electrodes and recorded under

undisturbed conditions for 48 h. During the light but not the dark phase, Ca_V3.DKO mice spent, on average, more time in NREM sleep and less time in waking, as compared to wild-type mice (Figure 5A). However, inspection of sleep bout length revealed that NREM sleep episodes of intermediate duration (32-252 s) occurred more frequently in Ca_V3.DKO mice at the expense of long episodes (> 252 s) ($F_{(1.0, 14.4)} = 7.8$, $P < 0.05$; Figure 5B). By contrast, no alterations were found in episode length and global time spent in REM sleep ($F_{(1.2, 16.3)} = 1.89$, $P > 0.05$; Figure 5A, B) or in the number of transitions from NREM to REM sleep (per hour of NREM sleep: 6.0 ± 0.5 in wild-type vs. 5.8 ± 0.4 in Ca_V3.DKO mice, $P > 0.05$). The changes in NREM sleep architecture appeared to be counterbalanced by alterations in waking episodes. Ca_V3.DKO mice spent more time in brief and intermediate periods of wakefulness (< 32 s, 32-124 s, $F_{(1.1, 14.7)} = 12.1$, $P < 0.01$), and, interestingly, NREM sleep episodes were more frequently interrupted by microarousals (per h of NREM sleep: 13 ± 1 microarousals in wild-type vs. 17 ± 1 microarousals in Ca_V3.DKO mice, $P < 0.01$, Figure 6A). Thus, although Ca_V3.DKO mice spent globally more time in NREM sleep episodes, these were of shorter duration, and sleep was generally more disrupted by short awakenings.

Next, we examined EEG power spectra of NREM and REM sleep. Absolute values of NREM sleep EEG power did not significantly differ between genotypes, although Ca_V3.DKO mice appeared to show an increase in the low-frequency range (slow-wave activity, SWA, 0.75-4 Hz) during both light and dark phase ($P = 0.22$ for the light phase, $P = 0.06$ for the dark phase; Figure 5C). To examine the relative contribution of specific spectral frequencies to the global EEG profile, and to account for inter-individual variations in EEG signal amplitude, we compared percentage EEG power values obtained by normalizing each frequency bin to the total power for each behavioral state (Figure 5D). The EEG profile of NREM sleep was significantly different in Ca_V3.DKO mice ($F_{(1.3, 18.1)} = 6.94$, $P < 0.05$) and, in particular, a marked reduction occurred across the whole σ frequency range (10-15 Hz: 0.57 ± 0.03% in wild-type vs. 0.41 ± 0.01% in Ca_V3.DKO mice, $P < 0.01$, *post hoc* unpaired *t*-test). A compromised spindle rhythmogenesis was also found when EEG power dynamics were analyzed at transitions between NREM and REM sleep, which are spindle-rich periods.[17, 25] In the NREM sleep epochs preceding REM sleep, σ power typically exhibits a surge, which is accompanied by a decrease in δ

power, indicative of reduced sleep depth. In Ca_V3.DKO mice, the surge in σ power was strongly diminished (144 ± 5% in wild-type vs. 123 ± 2% in Ca_V3.DKO mice, $P < 0.01$, Figure 5E). In contrast to the changes in σ power, relative EEG power in the low-frequency range was globally unaltered (0.75-4 Hz: 3.0 ± 0.1% in wild-type vs. 3.2 ± 0.1% in Ca_V3.DKO mice, $P > 0.05$). Interestingly, however, a significant increase was obtained when the higher range of δ frequencies was considered (2-4 Hz: 3.2 ± 0.1% in wild-type vs. 3.6 ± 0.1% in Ca_V3.DKO mice, $P < 0.05$).

The normalized EEG power spectrum of REM sleep was globally unaltered in Ca_V3.DKO mice ($F_{(1.6, 22.0)} = 3.3$, $P > 0.05$; Figure 5D). A slight increase in the higher range of δ frequencies occurred also during REM sleep (2-4 Hz: 1.70 ± 0.11% in wild-type vs. 1.93 ± 0.03% in Ca_V3.DKO mice, $P = 0.07$). A difference in SWA was also visible for absolute values of REM sleep EEG power ($P < 0.01$ for both phases; Figure 5C).

Absolute values of waking EEG power exhibited a general increase across frequency bands during both light and dark phase ($P < 0.01$ for both phases; Figure 6B). However, the relative contribution of the different frequency bands to the normalized power spectra was comparable ($F_{(2.9, 41.2)} = 1.94$, $P > 0.05$), with the exception of the frequency ranges corresponding to the α (8-12 Hz) and the β (12-20 Hz) band that displayed, on average, a significant reduction (8-12 Hz and 12-20 Hz: 0.89 ± 0.05% and 0.29 ± 0.01% in wild-type vs. 0.70 ± 0.02% and 0.25 ± 0.01% in Ca_V3.DKO mice, $P < 0.01$; Figure 6C).

Altogether, analysis of sleep EEG power indicates that *$Ca_V3.2$* and *$Ca_V3.3$* deletion induced a marked decrease in the relative contribution of the σ frequency range during NREM sleep, consistent with an impairment in sleep spindle rhythmogenesis. Additionally, the EEG power in the δ frequency range was augmented. Ca_V3.DKO mice spent more time in NREM sleep, but the predominance of short NREM sleep episodes together with the increase in microarousals indicates a more fragmented sleep architecture.

DISCUSSION

This work contributes to clarify the roles of Ca^{2+} channels for thalamic oscillations and sleep rhythms. In line with previous results, our data provide further evidence for a dominant role of $Ca_V3.3$ subtype in sustaining nRt low-threshold bursting and in activating the intrathalamic loop that underlies spindle pacemaking. In addition, our findings point at a modulatory function of the $Ca_V3.2$ subtype for nRt excitability, which might encode use-dependent changes of thalamic oscillations. Based on these observations, we propose that the co-expression of Ca_V32 and $Ca_V3.3$ subtypes in nRt underlies distinct aspects of this pacemaker structure in rhythmogenesis. In addition, the lack of low-threshold Ca^{2+} currents in Ca_V3.DKO mice excludes a functional contribution of the $Ca_V3.1$ subtype, although molecular analyses have also identified the presence of this isoform in nRt cells.[34]

Our study was largely based on a comparative analysis of single KOs for $Ca_V3.2$ channels and the DKO lacking both $Ca_V3.2$ and $Ca_V3.3$ channels. We found that removal of $Ca_V3.2$ channels only did not cause major alterations to nRt discharge, consistent with previous reports indicating a major contribution of $Ca_V3.3$ channels.[17, 18] In particular, low-threshold oscillatory bursting typical for NREM sleep rhythms, such as sleep spindles, was largely preserved in $Ca_V3.2$KO mice, and the underlying T-currents were comparable to wild-type levels.

We have analyzed cell excitability by applying somatic voltage steps, which might amplify the activation of proximal Ca_V3 channels and underestimate the contribution of distal compartments, especially in the case of the elongated dendrites of nRt neurons.[35] Are $Ca_V3.2$ channels preferentially located in distal dendritic branches? T-currents in nucleated patches from younger mice were shown to display higher Ni^{2+} sensitivity and faster inactivation kinetics than whole-cell T-currents, indicating that, at least during development, $Ca_V3.2$ channels are mainly located at proximal sites.[27]

We have further characterized the capability of Ca_V3 channels to generate nRt discharge when synaptically recruited. Upon stimulation of glutamatergic inputs onto nRt, bIPSCs could still be evoked in TC cells of $Ca_V3.2$KO mice, although with a reduced charge transfer, whereas this form of GABAergic transmission was impaired by *$Ca_V3.3$* ablation.[17] Synaptic recruitment of $Ca_V3.3$ channels

is hence obligatory for bIPSC generation, whereas $Ca_V3.2$ channels additionally appears to boost synaptic transmission mediated through burst discharge. A modulatory function for $Ca_V3.2$ channels, as opposed to a constitutive function of the dominating $Ca_V3.3$ channels, would be consistent with the well-documented sensitivity of the $Ca_V3.2$ channel to redox agents and to intracellular kinases[19] and might be important for use-dependent regulation of thalamocortical oscillations. An interesting open question is whether distinct Ca_V3 channel subunits are differentially recruited by cortical and thalamic glutamatergic inputs impinging onto nRt dendrites, thus modulating the feed-forward inhibition of TC cells in a subtype-specific manner.

Whereas Cav3.3-KO nRt cells showed a residual low-threshold Ca^{2+} spike carried by $Ca_V3.2$ channels,[17] Ca_V3.DKO mice displayed a complete lack of dendritic T-currents and rebound oscillatory bursting. This resulted in the abolishment of bIPSCs in TC cells, predicting disturbances in thalamic rhythms.[28] The striking effects on nRt excitability and intrathalamic synaptic transmission prompted us to examine the EEG sleep profile of Ca_V3.DKO mice. Corroborating our previous studies on the role of $Ca_V3.3$ channels in σ power, we find again a marked decrease in the σ power surge when both Ca_V3 channel subtypes are lacking. Additionally, Ca_V3.DKO mice also showed a reduced σ band in the normalized NREM sleep power spectrum. This suggests a more pronounced impairment in sleep spindle rhythmogenesis, as compared to $Ca_V3.3$KO mice, which is consistent with the full disappearance of bIPSCs in the DKOs. Additionally, in Ca_V3.DKO mice, the EEG-related phenotype was not specific to the σ range, but extended to EEG power between 2-4 Hz, belonging to the δ band, which was augmented. As a result, the balance between intrathalamic networks, providing the basis for sleep spindles, and thalamocortical circuitry, implicated in SWA, is affected more severely in the Ca_V3.DKO mice. Indeed, it has been previously shown that σ and δ power are negatively correlated during NREM sleep,[36-38] which was explained by a greater extent of membrane hyperpolarization of TC cells during δ rhythm generation in deep NREM sleep that precluded spindle rhythmicity. This current work now observes such a σ-δ power opposition through genetic means and suggests that the level of nRt excitability through Ca_V3 channels and the resulting bIPSC generation is a decisive factor for the σ/δ ratio apparent in the EEG.

Contrary to what would be expected from studies on pharmacological blockade of $GABA_AR$-mediated transmission in thalamic nuclei, Ca_V3.DKO mice did not display aberrant hypersynchronous rhythms, such as the 3 Hz spike-and-wave discharge.[28, 39] The emergence of these pathological oscillations was explained by a disinhibition of thalamic nuclei.[39, 40] Such hyperoscillations did not take place in the Ca_V3.DKO mice because GABAergic transmission in intrathalamic circuitry was not fully abolished, and some level of inhibition through tonic nRt discharge remained. Nevertheless, the imbalance between glutamatergic and GABAergic input onto TC cells in Ca_V3.DKO mice could favor intrinsic rhythmicity of TC neurons in the δ range at the expense of 10 Hz-nRt-TC reverberations.

The minor alterations in the θ frequency band during REM sleep are consistent with the evidence for the expression of $Ca_V3.2$ channels in the hippocampus and the detrimental consequences of *$Ca_V3.2$* ablation for hippocampal-related behavior and synaptic plasticity.[10, 41-43]

Despite the augmented contribution of δ waves, sleep was more fragmented in Ca_V3.DKO mice. These mice spent globally more time in NREM sleep than wild-type animals, but in episodes of shorter duration. The concomitant increase in waking bouts of short duration and the higher occurrence of microarousals support the conclusion that Ca_V3.DKO mice experienced a more fragmented sleep, which is consistent with the well-established link between spindles and sleep consolidation.[31] These data also support the view that manipulation of spindles can alter sleep architecture independently of δ waves, as previously reported in mice with a genetic overexpression of small-conductance type 2 K^+ channels, which improved sleep quality without altering SWA.[44]

Altogether, deletion of the additional source of low-threshold Ca^{2+} spike in nRt cells aggravated the sleep phenotype of $Ca_V3.3$KO mice, indicating a role of $Ca_V3.2$ channels in boosting nRt cell excitability and rhythmogenesis. Thus, the Ca_V3.DKO mice might represent a valuable model to study the involvement of nRt rhythmogenesis in pathophysiology, as already reported in the case of absence epilepsy.[26] The clinical relevance of Ca_V3.DKO mice remains a subject of further studies. Intriguingly, the deficits in sleep spindles strongly hint at the presence of a schizophrenic endophenotype.[45]

ACKNOWLEDGEMENTS

We are grateful to Kevin P Campbell for the permission of using the $Ca_V3.2$ knock-out mouse line, and to Heinz Beck for providing animal breeders. We thank Laura MJ Fernandez for help with data analysis and Thi Dung Hau Iuliano-Dao for mouse genotyping. This work was supported by the Swiss National Science Foundation (Ambizione grant PZ00P3_136761 to S.A. and grant 31003A-146244 to A.L.) and Etat de Vaud.

FIGURE LEGENDS

Figure 1 – Lack of overt changes in passive properties and tonic discharge of nRt cells of $Ca_V3.2KO$ and $Ca_V3.DKO$ mice. (**A**) Box-and-whisker plots with values of resting membrane potential (V_{rmp}), membrane capacitance (C_m) and input resistance (R_i) of nRt cells from wild-type (WT, n = 11), $Ca_V3.2KO$ (n = 9) and $Ca_V3.DKO$ (n = 9) mice. The midline in each box represents the median, the whiskers are 10th and 90th percentiles. (**B**) Left, representative current responses to hyperpolarizing voltage steps from -60 mV for all genotypes. Inset: protocol. Right, steady-state current (I_{ss}) for WT (n = 10), $Ca_V3.2KO$ (n = 9) and $Ca_V3.DKO$ (n = 9) nRt cells over a range of voltages. (**C**) Top, representative tonic discharges in WT, $Ca_V3.2KO$ and $Ca_V3.DKO$ nRt cells elicited by positive current injections from -70 mV. Bottom, average discharge frequency of tonic action potentials (APs) during the 400 ms over a range of positive currents injected (WT, n = 9; $Ca_V3.2KO$, n = 8; $Ca_V3.DKO$, n = 9; P > 0.05). Inset: voltage-clamp protocol.

Figure 2 – Suppression of oscillatory low-threshold bursting in nRt cells from $Ca_V3.DKO$ mice. (**A**) Representative traces of low-threshold bursting in WT, $Ca_V3.2KO$ and $Ca_V3.DKO$ nRt cells elicited at the offset of negative current injections from different membrane potentials. (**B**) Expanded traces from (**A**) at -70 mV. Inset: current-clamp protocol. (**C**) Number of low-threshold Ca^{2+} spikes and (**D**) number of action potentials (APs) during the first burst in WT (n = 10), $Ca_V3.2KO$ (n = 9), and $Ca_V3.DKO$ (n = 9) mice.

Figure 3 – Abolishment of low-threshold Ca^{2+} currents in nRt cells from $Ca_V3.DKO$ mice. (**A**) Top, isolated low-threshold Ca^{2+} currents elicited by depolarizing steps from -100 mV in WT, $Ca_V3.2KO$ and $Ca_V3.DKO$ nRt cells. Bottom, representative traces scaled to peak and bar graph showing mean values for decay time constant ($\tau_{w,\ decay}$) from WT and $Ca_V3.2KO$ (WT, n = 9; $Ca_V3.2KO$, n = 8; P = 0.07). Inset: voltage-clamp protocol. (**B**) T-current density for all genotypes (left) and activation curve (right) of the T-currents for WT and $Ca_V3.2KO$ with estimated V_{half} (WT: -71.1 ± 1.0 ms, n = 9; $Ca_V3.2KO$: -69.8 ± 1.7 mV, n = 8; P > 0.05). In $Ca_V3.DKO$ mice, no detectable T-currents were generated across the whole range of voltage steps (n = 9).

Figure 4 – Consequences of $Ca_V3.2$ and $Ca_V3.3$ channel deletion for nRt-TC GABAergic transmission. (**A**) Top, representative traces of rebound bursting elicited by hyperpolarizing current injections discharges in TC neurons held at -70 mV. Inset: current-clamp protocol. Bottom left, expanded traces shown in (**A**) for a -150 pA step of current injection. Bottom right, the number of action potentials per burst across a range of injected current did not change between genotypes (WT, n = 9, $Ca_V3.2$KO, n = 6, Ca_V3.DKO, n = 6; P > 0.05). (**B**) Left, example traces of evoked IPSCs recorded in TC cells at -30 mV upon electrical stimulation in the internal capsule. Inset, recording configuration showing site of stimulation in the internal capsule while recording from a TC cell in the ventrobasal nucleus (VB). Right, charge transfer across a range of stimulus intensities for all genotypes showing a minor and a strong decrease in the $Ca_V3.2$KO and Ca_V3.DKO mice, respectively, compared to WT animals. Inset shows mean responses to higher stimulus intensities (250-300 µA) (WT, n = 7, $Ca_V3.2$KO n = 8; Ca_V3.DKO, n = 7; one-way ANOVA, P < 0.05; ** P < 0.01,* P < 0.05, *post hoc* unpaired *t*-test).

Figure 5 – EEG sleep profile of Ca_V3.DKO mice. (**A**) Time spent in wake, NREM and REM sleep, expressed in % of 12 h and separated for light and dark period, for WT (n = 8) and Ca_V3.DKO (n = 8) mice. During the light phase, Ca_V3.DKO showed an increased amount of NREM sleep, while waking was reduced (state x genotype interaction: $F_{(1.2, 16.2)} = 7.73$, P < 0.05, * P < 0.05 *post hoc* unpaired *t*-test). No change occurred during the dark phase ($F_{(1.0, 14.6)} = 0.44$, P > 0.05). (**B**) Cumulative distributions of NREM and REM sleep episode duration pooled for light and dark phase. Statistical significance was tested with K-S statistics. Insets, histograms of time spent in short, intermediate and long episodes per hour of corresponding sleep (duration x genotype interaction: $F_{(1.0, 14.4)} = 7.8$, P < 0.05 for NREM sleep and $F_{(1.2, 16.3)} = 1.89$, P > 0.05 for REM sleep ; * P < 0.05, *post hoc* unpaired *t*-test). (**C**) Mean absolute power of relevant frequency bands during NREM or REM sleep separated for light and dark phase (SWA (0.75 - 4 Hz), σ (10 - 15 Hz) and θ (5 - 8 Hz); * P < 0.05, ** P < 0.01, unpaired *t*-test). (**D**) Normalized EEG power spectrum between 0.75 and 25 Hz for NREM (left) and REM (right) sleep. Red and orange lines on the x axes delineate intervals of frequency with a significant difference between genotypes, with P < 0.01 and < 0.05, respectively, tested with *post hoc* unpaired *t*-test after repeated measures ANOVA (genotype x frequency interaction: $F_{(1.3, 18.1)} = 6.94$, P < 0.05 for NREM sleep and

$F_{(1.6, 22.0)} = 3.3$, $P > 0.05$ for REM sleep). Dotted lines indicate frequency ranges for SWA (0.75 - 4 Hz), σ (10 - 15 Hz) and θ (5 - 8 Hz) bands used for the mean values presented in the bar graphs in the insets (** $P < 0.01$, unpaired *t*-test). (**E**) Left, examples of σ band-pass-filtered EEG recordings containing NREM-to-REM sleep transitions (occurring at time zero). Bar graph represents mean peak values of σ power before REM sleep onset (** $P < 0.01$, unpaired *t*-test). Right, color-coded heat maps of % EEG power between 0.75 and 25 Hz in 0.25 Hz bins averaged for all NREM-to-REM sleep transitions in WT (n = 8) and Ca_V3.DKO (n = 8) mice during light and dark phase. White dashed lines at zero indicate REM sleep onset. Data are normalized to the mean power from -3 to -1 min before the transition.

Figure 6 – Wake EEG profile of Ca_V3.DKO mice. (**A**) Top, cumulative distributions of wake episode durations during both light and dark phase. Statistical significance was tested with K-S statistics. Inset, histogram showing time spent in short, intermediate and long episodes per hour of wake (duration x genotype: $F_{(1.1, 14.7)} = 12.1$, $P < 0.01$; * $P < 0.05$, ** $P < 0.01$ *post hoc* unpaired *t*-test). Bottom, number of microarousals per hour of NREM sleep in WT and Ca_V3.DKO mice (** $P < 0.01$). (**B**) Mean absolute power of relevant frequency bands separated for light and dark phase (SWA (0.75 - 4 Hz), θ (5 - 8 Hz); * $P < 0.05$, ** $P < 0.01$, unpaired *t*-test). (**C**) Normalized EEG spectral power between 0.75 and 25 Hz during waking (genotype x frequency interaction: $F_{(2.9, 41.2)} = 1.94$, $P > 0.05$). Inset, mean values of normalized EEG power in the frequency range 8 - 20 Hz for WT and Ca_V3.DKO (** $P < 0.01$, unpaired *t*-test).

REFERENCES

1. Beenhakker MP, Huguenard JR. Neurons that fire together also conspire together: is normal sleep circuitry hijacked to generate epilepsy? Neuron 2009;62:612-32.

2. Crunelli V, Cope DW, Hughes SW. Thalamic T-type Ca^{2+} channels and NREM sleep. Cell Calcium 2006;40:175-90.

3. Cueni L, Canepari M, Adelman JP, Lüthi A. Ca^{2+} signaling by T-type Ca^{2+} channels in neurons. Pflügers Arch 2009;457:1161-72.

4. Ly R, Bouvier G, Schonewille M, et al. T-type channel blockade impairs long-term potentiation at the parallel fiber-Purkinje cell synapse and cerebellar learning. Proc Natl Acad Sci U S A 2013;110:20302-7.

5. Otsu Y, Marcaggi P, Feltz A, et al. Activity-dependent gating of calcium spikes by A-type K^+ channels controls climbing fiber signaling in Purkinje cell dendrites. Neuron 2014;84:137-51.

6. Egger V, Svoboda K, Mainen ZF. Dendrodendritic synaptic signals in olfactory bulb granule cells: local spine boost and global low-threshold spike. J Neurosci 2005;25:3521-30.

7. Becker AJ, Pitsch J, Sochivko D, et al. Transcriptional upregulation of $Ca_V3.2$ mediates epileptogenesis in the pilocarpine model of epilepsy. J Neurosci 2008;28:13341-53.

8. Shin HS, Cheong EJ, Choi S, Lee J, Na HS. T-type Ca^{2+} channels as therapeutic targets in the nervous system. Curr Opin Pharmacol 2008;8:33-41.

9. Perez-Reyes E. Molecular physiology of low-voltage-activated T-type calcium channels. Physiol Rev 2003;83:117-61.

10. Talley EM, Cribbs LL, Lee JH, Daud A, Perez-Reyes E, Bayliss DA. Differential distribution of three members of a gene family encoding low voltage-activated (T-type) calcium channels. J Neurosci 1999;19:1895-911.

11. Liu XB, Murray KD, Jones EG. Low-threshold calcium channel subunit $Ca_V3.3$ is specifically localized in GABAergic neurons of rodent thalamus and cerebral cortex. J Comp Neurol 2011;519:1181-95.

12. Fuentealba P, Steriade M. The reticular nucleus revisited: intrinsic and network properties of a thalamic pacemaker. Prog Neurobiol 2005;75:125-41.

13. Anderson MP, Mochizuki T, Xie J, et al. Thalamic $Ca_V3.1$ T-type Ca^{2+} channel plays a crucial role in stabilizing sleep. Proc Natl Acad Sci U S A 2005;102:1743-8.

14. Lee J, Kim D, Shin HS. Lack of delta waves and sleep disturbances during non-rapid eye movement sleep in mice lacking $a1_G$-subunit of T-type calcium channels. Proc Natl Acad Sci U S A 2004;101:18195-9.

15. Dossi RC, Nuñez A, Steriade M. Electrophysiology of a slow (0.5-4 Hz) intrinsic oscillation of cat thalamocortical neurones *in vivo*. J Physiol 1992;447:215-34.

16. Leresche N, Jassik-Gerschenfeld D, Haby M, Soltesz I, Crunelli V. Pacemaker-like and other types of spontaneous membrane potential oscillations of thalamocortical cells. Neurosci Lett 1990;113:72-7.

17. Astori S, Wimmer RD, Prosser HM, et al. The $Ca_V3.3$ calcium channel is the major sleep spindle pacemaker in thalamus. Proc Natl Acad Sci U S A 2011;108:13823-8.

18. Joksovic PM, Nelson MT, Jevtovic-Todorovic V, et al. $Ca_V3.2$ is the major molecular substrate for redox regulation of T-type Ca^{2+} channels in the rat and mouse thalamus. J Physiol 2006;574:415-30.

19. Iftinca MC, Zamponi GW. Regulation of neuronal T-type calcium channels. Trends Pharmacol Sci 2009;30:32-40.

20. Bourinet E, Alloui A, Monteil A, et al. Silencing of the $Ca_V3.2$ T-type calcium channel gene in sensory neurons demonstrates its major role in nociception. Embo J 2005;24:315-24.

21. Liao YF, Tsai ML, Chen CC, Yen CT. Involvement of the $Ca_V3.2$ T-type calcium channel in thalamic neuron discharge patterns. Mol Pain 2011;7:43.

22. Sekiguchi F, Kawabata A. T-type calcium channels: functional regulation and implication in pain signaling. J Pharmacol Sci 2013;122:244-50.

23. Chen CC, Lamping KG, Nuno DW, et al. Abnormal coronary function in mice deficient in $alpha_{1H}$ T-type Ca^{2+} channels. Science 2003;302:1416-8.

24. Cueni L, Canepari M, Luján R, et al. T-type Ca^{2+} channels, SK2 channels and SERCAs gate sleep-related oscillations in thalamic dendrites. Nat Neurosci 2008;11:683-92.

25. Franken P, Malafosse A, Tafti M. Genetic variation in EEG activity during sleep in inbred mice. Am J Physiol 1998;275:R1127-R37.

26. Lee SE, Lee J, Latchoumane C, et al. Rebound burst firing in the reticular thalamus is not essential for pharmacological absence seizures in mice. Proc Natl Acad Sci U S A 2014;111:11828-33.

27. Joksovic PM, Bayliss DA, Todorovic SM. Different kinetic properties of two T-type Ca^{2+} currents of rat reticular thalamic neurones and their modulation by enflurane. J Physiol 2005;566:125-42.

28. Rovó Z, Mátyás F, Barthó P, et al. Phasic, nonsynaptic GABA-A receptor-mediated inhibition entrains thalamocortical oscillations. J Neurosci 2014;34:7137-47.

29. Herd MB, Brown AR, Lambert JJ, Belelli D. Extrasynaptic $GABA_A$ receptors couple presynaptic activity to postsynaptic inhibition in the somatosensory thalamus. J Neurosci 2013;33:14850-68.

30. Sun YG, Wu CS, Renger JJ, Uebele VN, Lu HC, Beierlein M. GABAergic synaptic transmission triggers action potentials in thalamic reticular nucleus neurons. J Neurosci 2012;32:7782-90.

31. Astori S, Wimmer RD, Lüthi A. Manipulating sleep spindles - expanding views on sleep, memory, and disease. Trends Neurosci 2013;36:738-48.

32. McCormick DA, Bal T. Sleep and arousal: thalamocortical mechanisms. Annu Rev Neurosci 1997;20:185-215.

33. Steriade M. Grouping of brain rhythms in corticothalamic systems. Neuroscience 2006;137:1087-106.

34. McKay BE, McRory JE, Molineux ML, et al. Ca_V3 T-type calcium channel isoforms differentially distribute to somatic and dendritic compartments in rat central neurons. Eur J Neurosci 2006;24:2581-94.

35. Warren RA, Jones EG. Maturation of neuronal form and function in a mouse thalamo-cortical circuit. J Neurosci 1997;17:277-95.

36. Nuñez A, Curro Dossi R, Contreras D, Steriade M. Intracellular evidence for incompatibility between spindle and delta oscillations in thalamocortical neurons of cat. Neuroscience 1992;48:75-85.

37. Uchida S, Maloney T, March JD, Azari R, Feinberg I. Sigma (12-15 Hz) and delta (0.3-3 Hz) EEG oscillate reciprocally within NREM sleep. Brain Res Bull 1991;27:93-6.

38. Vyazovskiy VV, Achermann P, Borbély AA, Tobler I. The dynamics of spindles and EEG slow-wave activity in NREM sleep in mice. Arch Ital Biol 2004;142:511-23.

39. Castro-Alamancos MA. Neocortical synchronized oscillations induced by thalamic disinhibition in vivo. J Neurosci 1999;19:RC27.

40. Paz JT, Bryant AS, Peng K, et al. A new mode of corticothalamic transmission revealed in the *Gria4*$^{-/-}$ model of absence epilepsy. Nat Neurosci 2011;14:1167-73.

41. Chen CC, Shen JW, Chung NC, Min MY, Cheng SJ, Liu IY. Retrieval of context-associated memory is dependent on the $Ca_V3.2$ T-type calcium channel. PLoS One 2012;7:e29384.

42. Chung NC, Huang YH, Chang CH, et al. Behavior training reverses asymmetry in hippocampal transcriptome of the *$Ca_V3.2$* knockout mice. PLoS One 2015;10:e0118832.

43. Gangarossa G, Laffray S, Bourinet E, Valjent E. T-type calcium channel $Ca_V3.2$ deficient mice show elevated anxiety, impaired memory and reduced sensitivity to psychostimulants. Front Behav Neurosci 2014;8:92.

44. Wimmer RD, Astori S, Bond CT, et al. Sustaining sleep spindles through enhanced SK2-channel activity consolidates sleep and elevates arousal threshold. J Neurosci 2012;32:13917-28.

45. Ferrarelli F, Tononi G. The thalamic reticular nucleus and schizophrenia. Schizophr Bull 2011;37:306-15.

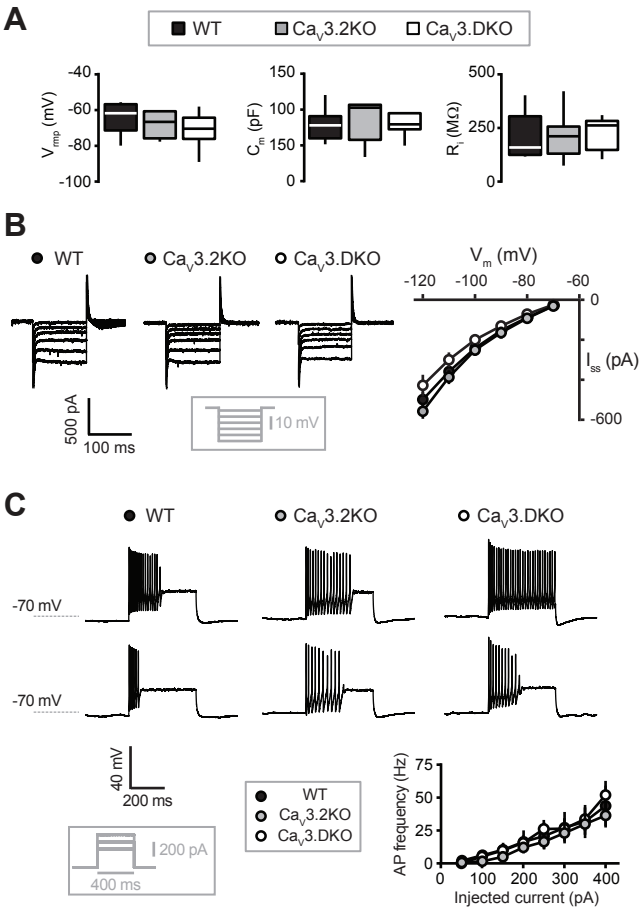
A
WT
CaV3.2KO
CaV3.DKO
Vrmp (mV)
-40
-60
-80
-100
Cm (pF)
150
100
150
0
Ri (MΩ)
500
250
0
B
WT
CaV3.2KO
CaV3.DKO
Vm (mV)
-120
-100
-80
-60
0
Iss (pA)
-600
500 pA
100 ms
10 mV
C
WT
CaV3.2KO
CaV3.DKO
-70 mV
-70 mV
40 mV
200 ms
200 pA
400 ms
WT
CaV3.2KO
CaV3.DKO
AP frequency (Hz)
75
50
25
0
0
100
200
300
400
Injected current (pA)

Figure 1

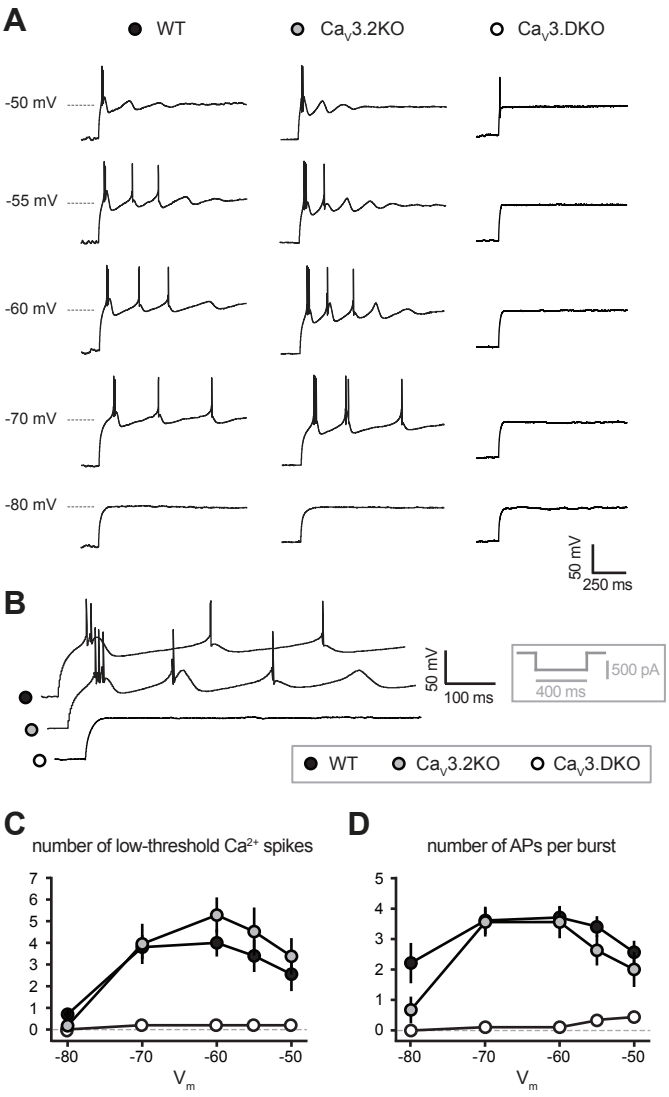
A
WT
Ca$_V$3.2KO
Ca$_V$3.DKO
-50 mV
-55 mV
-60 mV
-70 mV
-80 mV
50 mV
250 ms
B
50 mV
100 ms
500 pA
400 ms
WT
Ca$_V$3.2KO
Ca$_V$3.DKO
C
number of low-threshold Ca^{2+} spikes
V$_m$
D
number of APs per burst
V$_m$

Figure 2

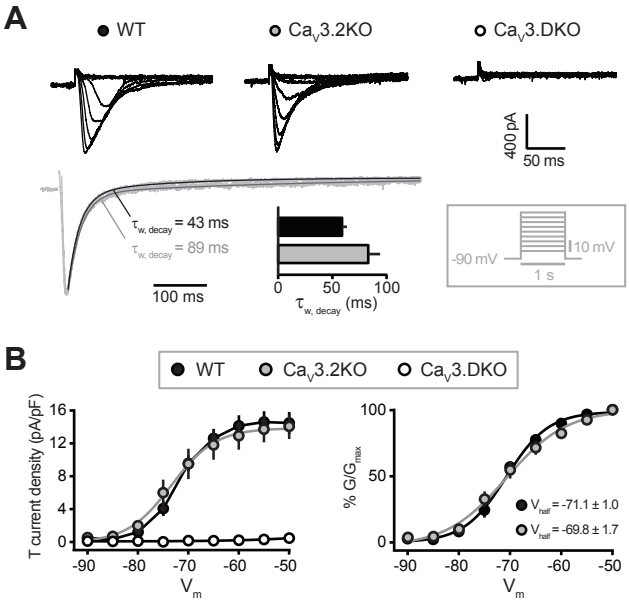
A
WT
Cav3.2KO
Cav3.DKO
400 pA
50 ms
τw, decay = 43 ms
τw, decay = 89 ms
100 ms
0
50
100
τw, decay (ms)
-90 mV
10 mV
1 s
B
WT
Cav3.2KO
Cav3.DKO
T current density (pA/pF)
16
12
8
4
0
-90
-80
-70
-60
-50
Vm
100
50
0
% G/Gmax
Vhalf = -71.1 ± 1.0
Vhalf = -69.8 ± 1.7

Figure 3

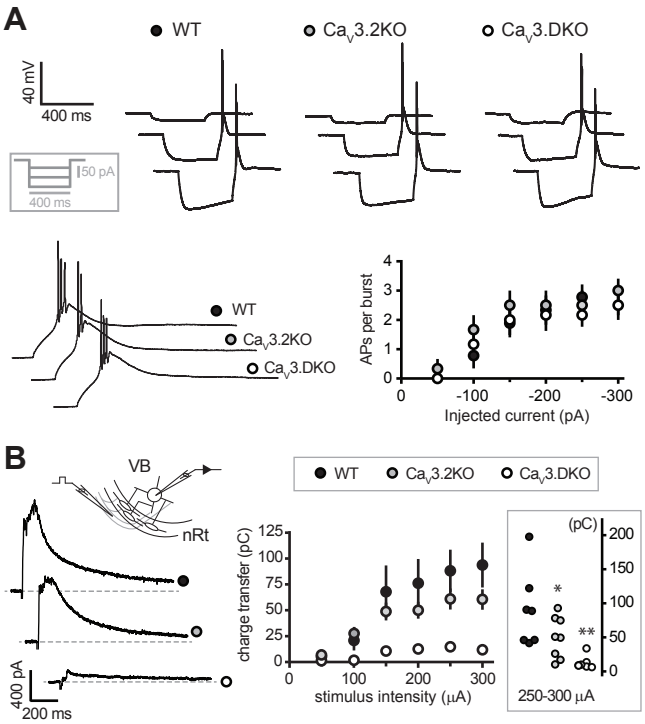
A
WT
Ca$_V$3.2KO
Ca$_V$3.DKO
40 mV
400 ms
50 pA
400 ms
WT
Ca$_V$3.2KO
Ca$_V$3.DKO
APs per burst
Injected current (pA)
B
VB
nRt
WT
Ca$_V$3.2KO
Ca$_V$3.DKO
charge transfer (pC)
stimulus intensity (μA)
(pC)
250-300 μA
400 pA
200 ms

Figure 4

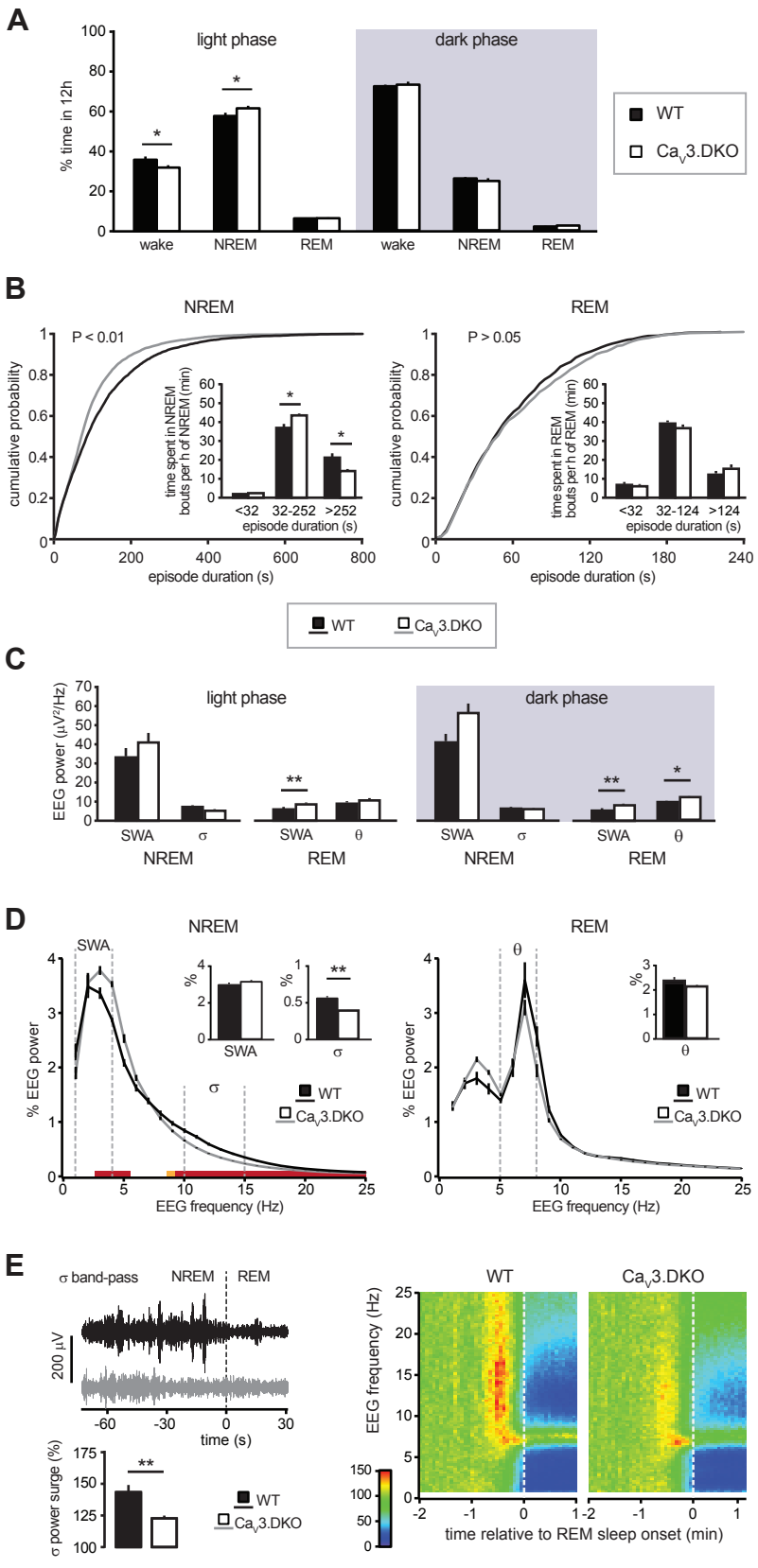
A
light phase
dark phase
% time in 12h
wake
NREM
REM
WT
Ca$_V$3.DKO
B
NREM
REM
P < 0.01
P > 0.05
cumulative probability
episode duration (s)
time spent in NREM bouts per h of NREM (min)
time spent in REM bouts per h of REM (min)
<32
32-252
>252
32-124
>124
C
EEG power (µV²/Hz)
SWA
σ
θ
D
% EEG power
EEG frequency (Hz)
E
σ band-pass
200 µV
time (s)
σ power surge (%)
EEG frequency (Hz)
time relative to REM sleep onset (min)

Figure 5

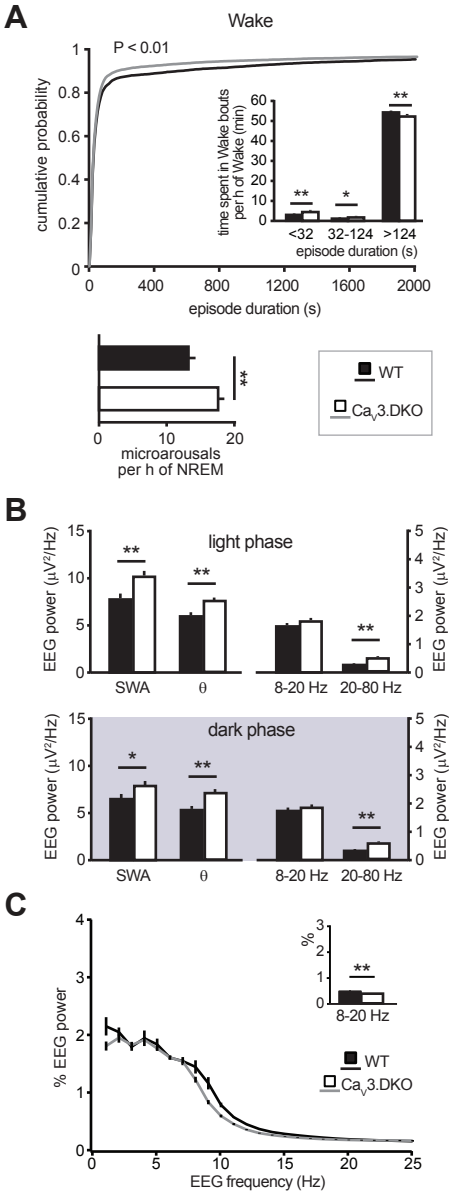
A
Wake
P < 0.01
cumulative probability
episode duration (s)
time spent in Wake bouts per h of Wake (min)
<32
32-124
>124
episode duration (s)
microarousals per h of NREM
WT
Ca$_v$3.DKO
B
light phase
dark phase
EEG power (μV²/Hz)
SWA
θ
8-20 Hz
20-80 Hz
C
% EEG power
EEG frequency (Hz)
8-20 Hz
WT
Ca$_v$3.DKO

Figure 6